Sharma, S.; Garcia Tiscar, J.; Allport, JM.; Barrans, S.; Nickson, AK. (2021). Evolution of flow characteristics in a centrifugal compressor with an increase in operating speed. International Journal of Engine Research. 22(5):1592-1604. https://doi.org/10.1177/1468087420916606

Evolution of flow characteristics in a centrifugal compressor with an increase in operating speed

Sidharath Sharma[1], Jorge García-Tíscar[2], John M. Allport[1], Simon Barrans [1], and Ambrose K. Nickson[3]

Abstract

Developments in materials, manufacturing and computing methods have catalysed the generation of efficient compressor designs with higher specific power outputs. Centrifugal compressors have become pervasive in environments demanding a combination of higher power with smaller sizes such as unmanned aerial vehicles, micro gas turbines and turbochargers. These compressors are expected to perform optimally in a range of operational speeds and mass flow states with low acoustic emissions. The impact of operating speed on the flow and acoustic characteristics of a ported shroud compressor has been explored in this work. The operation of the open and blocked configurations of the compressor at the design and near surge points each of a lower and a higher speedline were numerically and experimentally investigated. Comparing the results, the model was shown to predict the operation of the compressor for both configurations at the investigated operating points satisfactorily in terms of both performance and dominant acoustic features. With an increase in the velocity and Mach number due to increased operational speed, changes in the flow behaviour in the inducer and diffuser were observed. An increase in operational speed was shown to generally increase the overall acoustic emission of the compressor for both configurations. The number of distinct tones in the acoustic output and their magnitude was also seen to be a function of operating speed.

Keywords

Compressor noise, SBES, Ported shroud, CFD, Aeroacoustics

Introduction

The specific power output of centrifugal compressors has increased over time due to the incorporation of innovative control technologies, specialised materials and sophisticated aerodynamic designs. These centrifugal machines are better suited for smaller sizes and operate in a wide range of rotating speed in a myriad of applications including helicopters, unmanned aerial vehicles, micro gas turbines, turbochargers, vacuum cleaners, hair dryers and even artificial heart pumps. In all these applications it is desirable for audible noise generation to be minimized and in particular, for potentially annoying tones to be avoided. As the change in sound power is proportional to the fifth or sixth power of the change in rotor tip speed, the acoustic emission from these small, high-speed, centrifugal compressors is a critical parameter for designers. In addition to a wide range of operational speed, these machines are also expected to deliver superior aerodynamic performance over a wide range of mass flow rates. This is often achieved by the use of ported shroud (PS)[1–4] casing treatments wherein the onset of surge is delayed by recirculating the low momentum fluid, that blocks the blade passage, back to the compressor inlet. The evolution of flow and noise characteristics in such a compressor is investigated in this work.

[1] Turbocharger Research Institute, University of Huddersfield, UK
[2] CMT – Motores Térmicos, Universitat Politècnica de València, Spain
[3] BorgWarner Turbo Systems Division, UK

Corresponding author:
Sidharath Sharma, Turbocharger Research Institute
University of Huddersfield, Queensgate, Huddersfield, HD1 3DH, UK.

Email: sidharath.sharma@hud.ac.uk

The numerical investigations by Christou[5], Semlitsch et al.[4] and Yang et al.[6] explored flow characteristics of the compressor over various mass flow states while the impact of ported shroud and operating speed on the acoustic emission was not considered. Zheng et al.[7,8] and Torregrosa et al.[9,10] experimentally investigated the flow instabilities and acoustic characteristics of the compressors without casing treatment. Furthermore, the impact of operating speed was not investigated. Recent attempts to understand the relationship between flow and acoustic features of a PS compressor are made by decomposing the numerical flow field using proper orthogonal decomposition[11,12] and dynamic mode decomposition[13] and the role of PS casing treatment in alleviating the broadband noise observed for near surge operation was shown.

The experimental acoustic investigations of Evans and Ward[14] and Trochon[15] focused on the broadband noise observed in the 1.5-3 kHz range. The work of Teng and Homco[16] and Figurella et al.[17] also studied the broadband noise present but in an inclusive frequency range of 4-12 kHz. The acoustic spectra of a centrifugal compressor comprises of tonal and broadband features[18]. Tonal features include Rotating Order (RO) tones or 'buzz-saw' tones[11,18] and Blade Pass Frequency (BPF) while broadband features include the so called 'whoosh' noise which is observed within the plane wave frequency range and Tip Clearance Noise (TCN)[18,19] seen beyond the plane wave frequency.

A direct approach for modelling in-duct compressor noise was demonstrated by Broatch et al.[13,20] wherein hydrodynamic and acoustic pressure fluctuations are calculated by directly solving the unsteady Navier-Stokes equations. This approach has been used in the work presented in this paper. Furthermore, an exhaustive evaluation of the various modelling parameters for predicting flow-induced noise in compressors is presented by Sharma et al.[21] emphasising the need for higher spatial and temporal resolution for scale-resolving turbulence formulations to yield accurate results. The literature on the acoustic impact of casing treatments is scarce, and the general perception[22,23] is that casing treatments deteriorate the acoustic spectra of compressors. Recent numerical and experimental studies[24–26] have shown the improvement offered by PS treatment in the acoustic spectra for near surge operation.

Although not explicitly studied, the general trend observed in the experimental work of Torregrosa et al.[27] and Dehner et al.[28] points towards an expected increase in the noise levels with the increase in operational speed of the compressor. The current investigation aims to understand the impact of the operating speed on the flow and acoustic characteristics of a compressor with and without PS using experimental and numerical methods.

Methodology

A compressor with a shroud, as shown in Fig. 1, was modelled both with the shroud ported and without ports in the shroud. These configurations are referred to as PS open and PS blocked respectively. The blocked configuration was realised by removing the PS slot in the open configuration. The behaviour of these compressor configurations operating at the 99 krpm (lower) speedline was compared with that at the 130 krpm (higher) speedline. The analysed operating

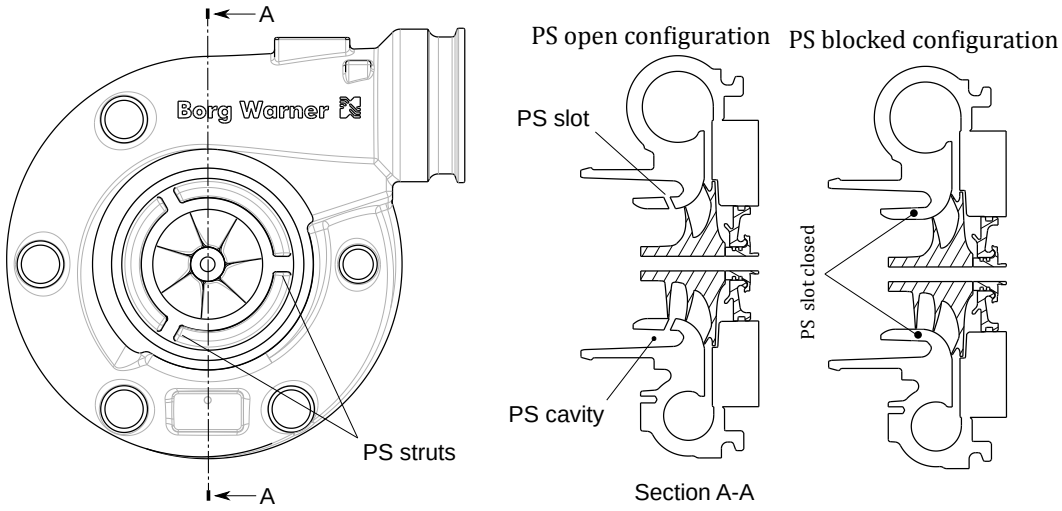

Figure 1. Drawing of the compressor along with sectional views of the open and blocked compressor configurations.

points are highlighted in the compressor maps presented in Fig. 2. These compressor maps are obtained from gas stand measurements and the surge points corresponds to the mild surge computed using a criterion based on experimental pressure fluctuations.

To quantify the impact of rotational speed, the operating points at two different speedlines must be aerodynamically and geometrically similar. Geometric similarity was assured as the same compressor configuration was used. Aerodynamic similarity between different operating points is normally assured by ensuring that the flow coefficients (ψ) * for those points is similar. It can be seen in Tab. 1 that at the design points, this is the case. However the flow coefficient at the near surge points changes significantly as speed is increased for both compressors.

Table 1. The values of flow coefficient (ψ) for the investigated design and near surge conditions of two speedlines.

Speedline	Configuration	Case	ψ [-]
99 krpm	PS open	Design	1.28
		Near surge	0.74
	PS blocked	Design	1.28
		Near surge	0.74
130 krpm	PS open	Design	1.3
		Near surge	1.04
	PS blocked	Design	1.3
		Near surge	1.12

Furthermore, the flow coefficient at the design points for the open and blocked configurations are similar across the speedlines, while for the near surge point, the flow coefficients values for the two configurations are only similar for the 99 krpm speedline. This implies that the impact of PS and operating speed on the flow and acoustic emission of the compressor operating at design conditions can be established by directly comparing the flow features and acoustic spectra of respective configurations across the speedlines. However, the impact of the PS on the near surge operation can only be established by comparing the near surge spectra of the two configurations operating at the 99 krpm speedline.

The impact of operating speed on the flow and acoustic characteristics of near surge point cannot be accurately quantified by comparing the near surge spectra of the two speedlines as the flow coefficients and thereby, aerodynamic conditions would be very different. This being said, the near surge spectra at the

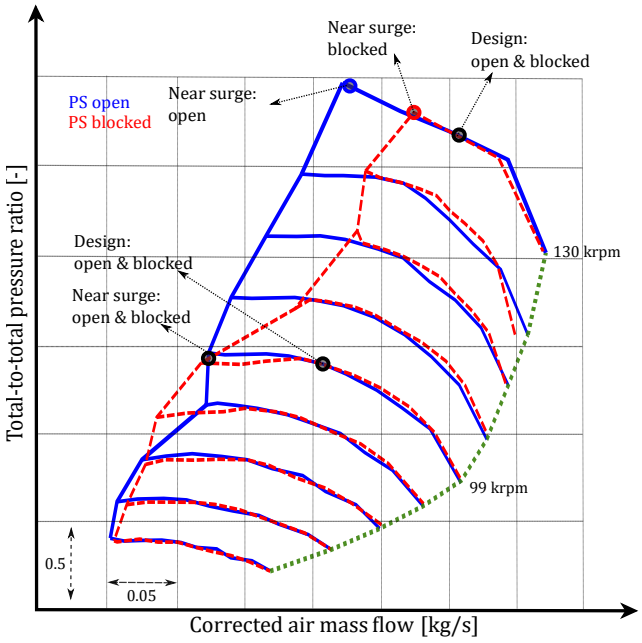

Figure 2. Compressor maps for the open and blocked configurations obtained from gas stand measurements, highlighting the investigated operating points on 99 krpm and 130 krpm speedline.

two speedlines can provide information on the evolution of the near surge acoustics with speed, fully realising that the changes in the acoustic characteristics are not solely down to the changes in the operational speed.

The commercial CFD coupled solver, ANSYS CFX[29] was used to obtain the numerical data. The noise generated by the impeller was quantified using virtual pressure probes positioned in the inducer and diffuser of the compressor as shown in Fig. 3. The pressure fluctuations derived from the flow solution, for the two pressure probes, were processed to obtain the spectral characteristics.

The complete lengths of the inlet and outlet ducts used in the measurement rig (see Fig. 4) were not included in the model because of computational intractability. Lengths equivalent to 4 cross-sectional diameters were modelled. This decreased the impact of the boundary conditions on the mean flow allowed possible flow instability propagating upstream of the impeller to be captured. Straight ducts were used to uncouple issues due to the PS from those caused by more realistic inlet geometries such as elbows[30], tapered ducts[31] etc.

The pressure spectra presented in terms of Power Spectral Density (PSD) were obtained using Welch's

* $\Psi = Q_{in}/U_{tip}A_{in}$ where Q_{in} is volumetric mass flow, U_{tip} is impeller tip speed and A_{in} is the area of the inducer

overlapped segmented averaging[32] of the pressure data with the number of blocks selected to achieve a frequency resolution of approximately 50 Hz. Further details on the numerical modelling and methodology have been presented in Sharma et al.[11,21].

Numerical configuration

A B2G turbocharger PS compressor provided by industrial partner BorgWarner was the subject of this investigation. The numerical configuration employed is described in detail in Sharma et al.[24] and was based on the Stress Blended Eddy Simulation (SBES)[33] turbulence formulation with 10 million cells and a timestep corresponding to a 4° rotation of the impeller per iteration. The limitations of this numerical set-up which are described in Sharma et al.[21] include the inability to accurately capture the overall levels and decay rates and accentuated tonal content. However, since this work focused on understanding the changes between two different operational states (speed) in the ranges sensitive to the human ear (0.5-10 kHz[34]), rather than the absolute values; the limitations of the approach can be accepted.

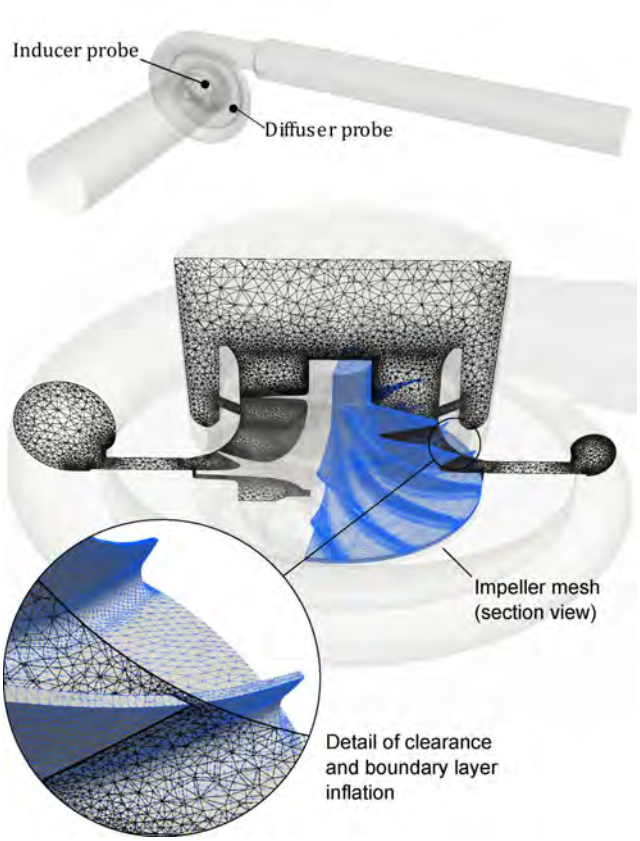

Figure 3. View of the computational domain showing a slice of the fluid mesh, the rotor surface mesh and the clearance between the blades and the shroud along with the boundary layer inflation. The location of inducer and diffuser virtual pressure probes are also shown.

The computational domain was spatially discretized by an unstructured polyhedral control volume created from the tetrahedral cells generated in ICEM CFD[35] by the vertex- centered numerical approach in ANSYS CFX[29]. The grid is shown in the Fig. 3. The impeller motion was modelled using the Rigid Body Motion (RBM) approach, also known as sliding mesh in which the mesh actually rotates every time-step at the transient rotor-stator interface[29]. A steady boundary condition, as a combination of the total pressure and total temperature at the inlet and mass flow rate at the outlet, was prescribed in this work.

Assessment of the numerical configuration

The ability of the numerical configuration to yield meaningful predictions was assessed by comparing the acoustic and performance characteristics predicted numerically with the corresponding experimental measurements. The performance measurements were performed at the gas stand testing facility at BorgWarner Turbo Systems, Bradford while the acoustic measurements were carried out in a flow bench facility hosted in CMT – Motores Térmicos. Compressor performance characteristics viz. total-to-total pressure ratio Π_{t-t} and isentropic efficiency η_s were computed from the measured thermodynamic variables of the state in accordance with Eq. 1 and Eq. 2.

$$\Pi_{t-t} = \frac{p_{out,0}}{p_{in,0}} \tag{1}$$

where $p_{in,0}$ and $p_{out,0}$ is the total pressure at the compressor inlet and outlet respectively.

$$\eta_s = \frac{T_{in,0}}{T_{out,0} - T_{in,0}} \left({\Pi_{t-t}}^{\gamma-1/\gamma} - 1 \right) \tag{2}$$

where $T_{in,0}$ and $T_{out,0}$ is the total temperature at the compressor inlet and outlet respectively while γ is the ratio of the specific heats.

Details on the gas stand measurement are described in Sharma et al.[11,36]. Schematic diagrams of the acoustic flow bench with the position of various sensors is shown in Fig. 4. The noise propagation to the ducts was measured using the pressure sensors positioned in the inlet and outlet ducts, while the noise generated by the impeller was measured using two miniaturised pressure probes positioned in the inducer and diffuser. Further details on the flow bench and measurement methodology

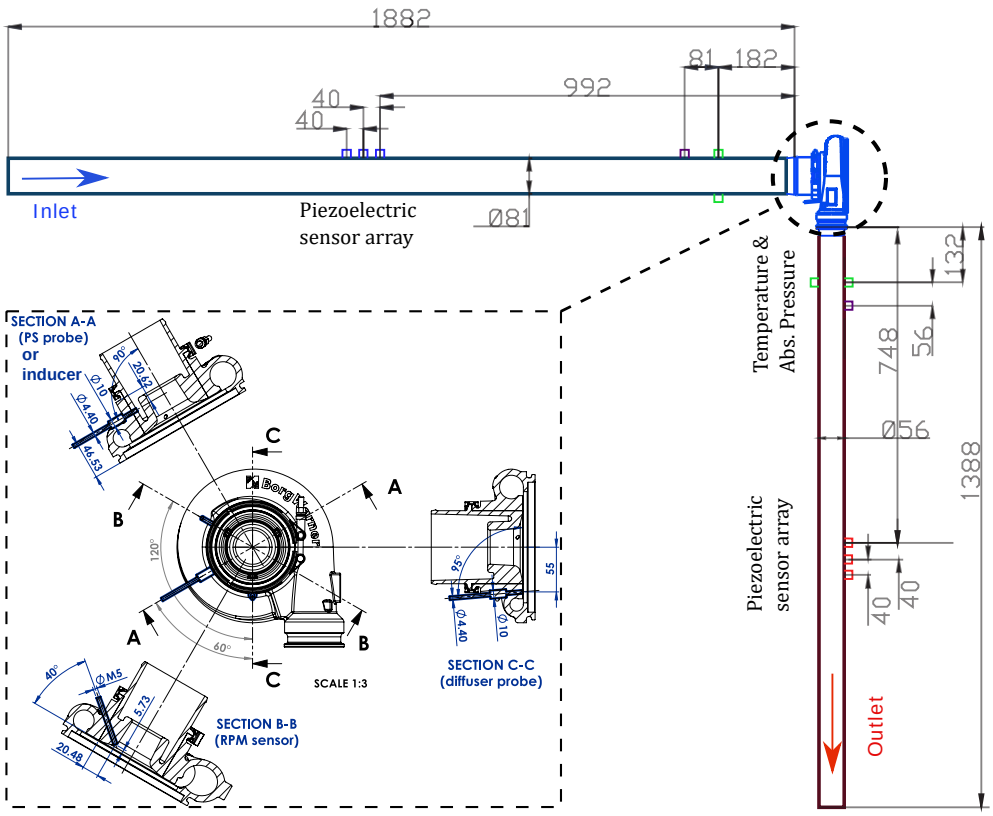

Figure 4. Experimental set-up used for acoustic measurements showing sensor positions. Dimensions in millimetres (mm).

Table 2. Performance characteristics Π_{t-t} and η_s of two configurations operating at 130 krpm and 99 krpm predicted by the numerical model are compared with the experimental measurements

Results	Configuration	Case	130 krpm				99 krpm			
			Π_{t-t} [-]	η_s [%]	ε_Π [%]	ε_η [%]	Π_{t-t} [-]	η_s [%]	ε_Π [%]	ε_η [%]
Experimental	PS open	Design	3.86	72.2	-	-	2.35	76.8	-	-
		Near surge	4.16	68.3	-	-	2.47	66.7	-	-
	PS blocked	Design	3.94	72.8	-	-	2.37	78.5	-	-
		Near surge	3.98	69.2	-	-	2.45	68.3	-	-
Numerical	PS open	Design	3.74	71.4	3.1	1.1	2.32	76.1	1	0.9
		Near surge	4	67.8	3.8	0.7	2.47	66.4	0.1	0.5
	PS blocked	Design	3.84	72.1	2.5	1	2.33	76.3	1.6	2.8
		Near surge	3.85	68.3	3.3	1.3	2.44	66	0.4	3.3

are presented in Sharma et al.[12,25]. The relative difference between experimental and numerical data was quantified using a relative deviation ε value, which for a generic variable ϕ with subscripts representing numerical (num) and experimental (exp) results, can be defined as

$$\varepsilon = \frac{|\phi_{\text{num}} - \phi_{\text{exp}}|}{\phi_{\text{exp}}} 100 \tag{3}$$

The performance parameters for the compressor along with the relative deviation from experimental values (Eq. 3) for the investigated configurations and operation are presented in Tab. 2. The deviation between the measured and predicted results are observed to be higher for the 130 krpm speedline relative to the 99 krpm speedline. This is expected as an adiabatic wall condition used in the numerical model would not capture the increased heat transfer effects. The impact of heat transfer would be significant at the higher operating speeds due to the increased temperature of compressed air and the hot-gasses driving the turbine. Nevertheless, the performance parameters are predicted within reasonable limits with the deviation from measured values in the range of ± 4 %.

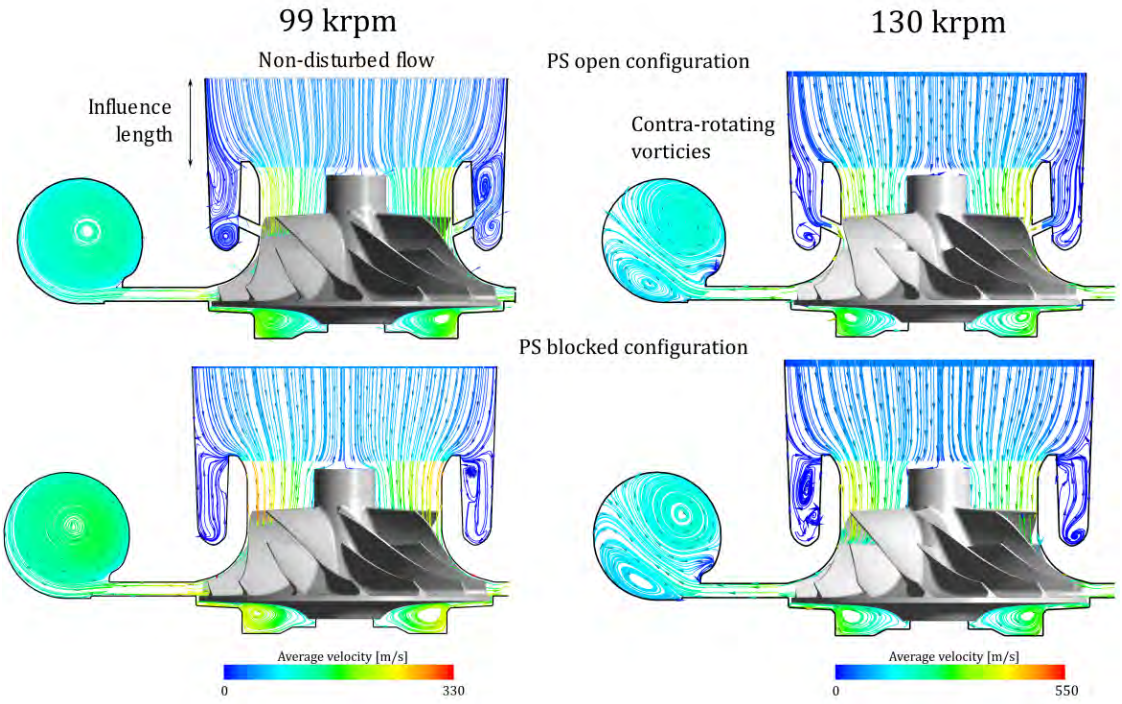

Figure 5. Flow field characteristics observed at the design operation of 99 krpm (top) and 130 krpm (bottom) speedlines for open (left) and blocked (right) compressor configurations at the impeller axis plane.

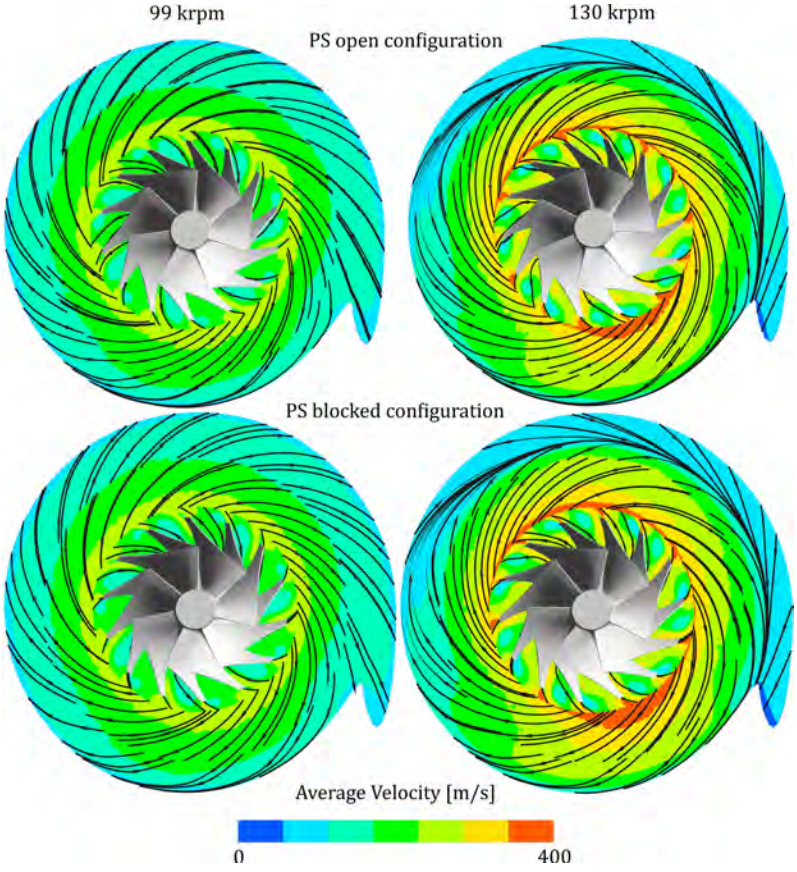

Figure 6. Flow field characteristics observed at the design operation of 99 krpm (left) and 130 krpm (right) speedlines for open (top) and blocked (bottom) compressor configurations at the mid-diffuser plane.

Noise evolution for design point operation

The impact of the operational speed on the flow and acoustic features for the open and blocked configurations of the compressor operating at the design operating conditions are discussed here.

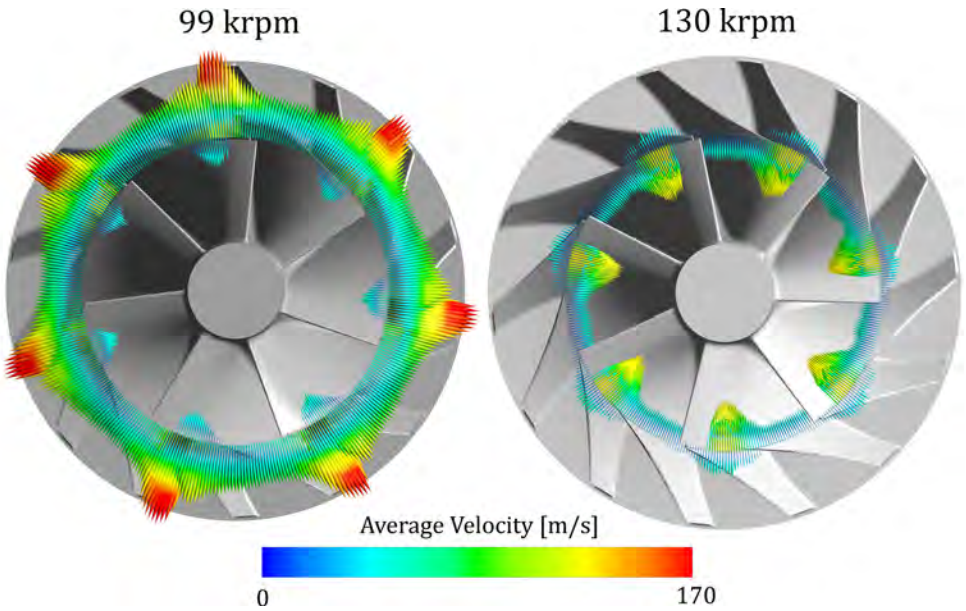

Figure 7. Velocity vectors at the PS slot for the design point of 99 krpm (left) and 130 krpm (right) speedline.

Flow features

The mean flow field on the axial plane of the two compressor configurations operating at the design conditions of the 99 krpm (top) and 130 krpm (bottom) speedlines are shown in Fig. 5. With the increase in operating speed, the expected increase in the velocity of the incoming flow is observed for both configurations. Although the flow features observed in the inlet and rotor region for the design conditions at the two speedlines are similar, the formation of contra rotating vortices can be observed in the volute of the higher speedline.

The contra rotating vortices are believed to be caused by the inability of the flow to follow the volute curvature due to higher swirl and velocity in the flow coming out of the impeller at the higher speedline. This can be clearly seen in the distribution of the flow exiting impeller into the diffuser as shown in Fig. 6. The flow in both open and blocked compressor configurations operating at 99 krpm is observed to smoothly travel from the trailing edge to the volute wall while for the 130 speedline, the flow is seen to impinge off the volute wall (right) and to interact with the oncoming flow leading to the formation of contra rotating vortices.

A smooth reduction of area caused by the PS cavity is observed for both speedlines and both configurations in Fig. 5. However, for the open PS case, the 'inverted-S' shape feature is not observed in the PS cavity for

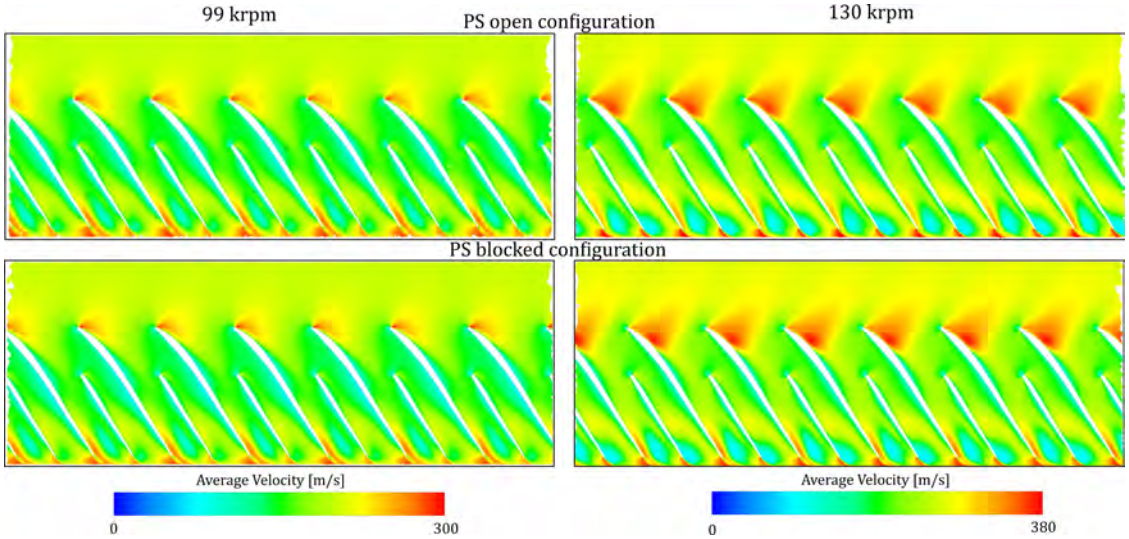

Figure 8. Midspan blade-to-blade views of average velocity for the open (top) and blocked (bottom) configuration of compressors operating at the respective design conditions of 99 krpm (left) and 130krpm (right) speedline.

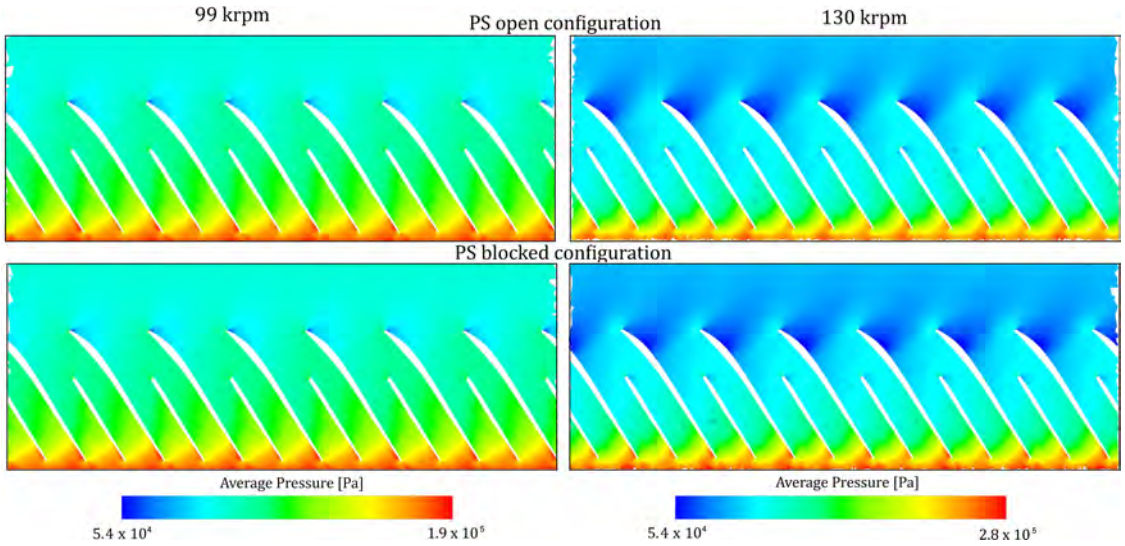

Figure 9. Midspan blade-to-blade views of average pressure for the open (top) and blocked (bottom) configuration of compressors operating at the respective design conditions of 99 krpm (left) and 130krpm (right) speedline.

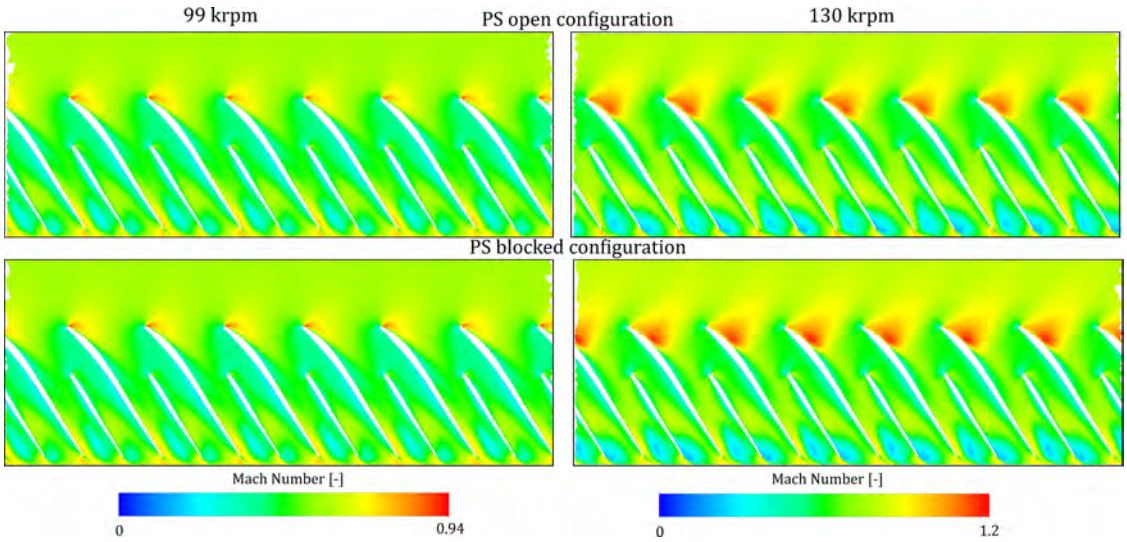

Figure 10. Midspan blade-to-blade views of average Mach number for the open (top) and blocked (bottom) configuration of compressors operating at the respective design conditions of 99 krpm (left) and 130krpm (right) speedline.

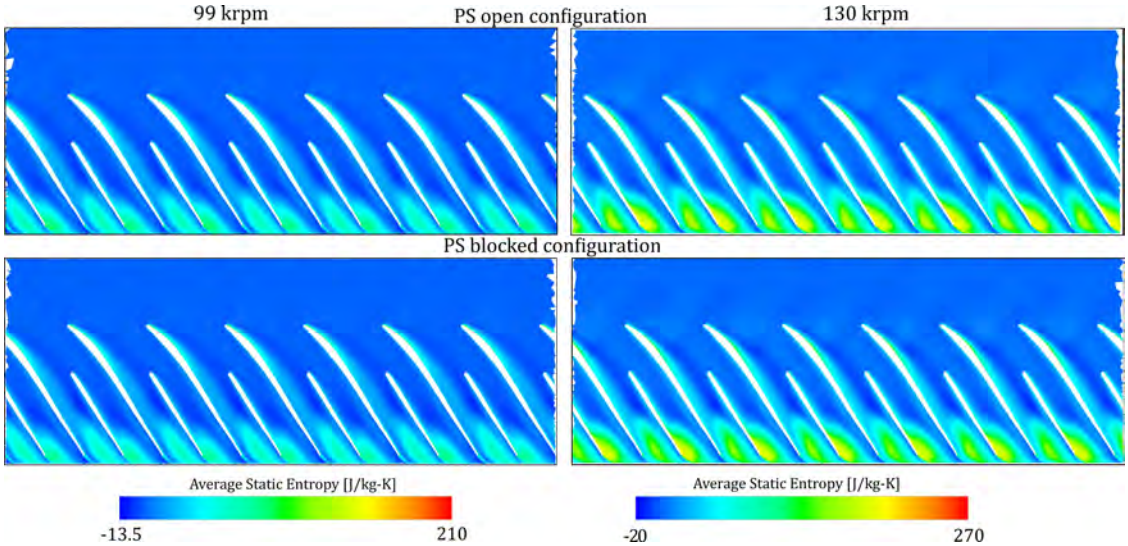

Figure 11. Midspan blade-to-blade views of average entropy generation for the open (top) and blocked (bottom) configuration of compressors operating at the respective design conditions of 99 krpm (left) and 130krpm (right) speedline.

the higher speedline. For the blocked PS case similar flow features are observed at the two speedlines. The 'push and pull'[11] of flow at the PS slot for the open configuration shows an interesting dynamics (see Fig. 7), wherein the flow distribution is primarily observed to be surge-like, i.e. pushed out of the impeller, for the lower speedline whereas at the higher operational speed, the flow behaviour is choke-like, i.e. pulled into the impeller. Furthermore, the fluid undergoing 'push and pull' at the PS slot and recirculating in the PS cavity is seen to be relatively reduced for higher speedline.

The distributions of velocity and pressure inside the impeller for the two speedlines are presented in Fig. 8 and Fig. 9 respectively. The expected increase in the amplitude of both velocity and pressure with an increase in the operating speed is observed. At a given operating speed point there is little difference between the blocked and open PS configurations in terms of both distribution and magnitude of either velocity or pressure.

The distribution of the Mach number at the rotor midspan (see Fig. 10) shows transonic-supersonic conditions for the higher speedline in contrast to subsonic-transonic conditions for the lower speedline for both blocked and open configurations with little difference between the configurations. This implies the presence of stronger shock waves at the 130 krpm speedline and thereby, intense RO tones are expected in the spectra of both open and blocked configurations . The generation of entropy is observed to be significantly higher for both configurations operating at 130 krpm as seen in Fig. 11. Therefore, operation at the higher speedline is expected to have higher losses in the impeller relative to the operation at the lower speedline.

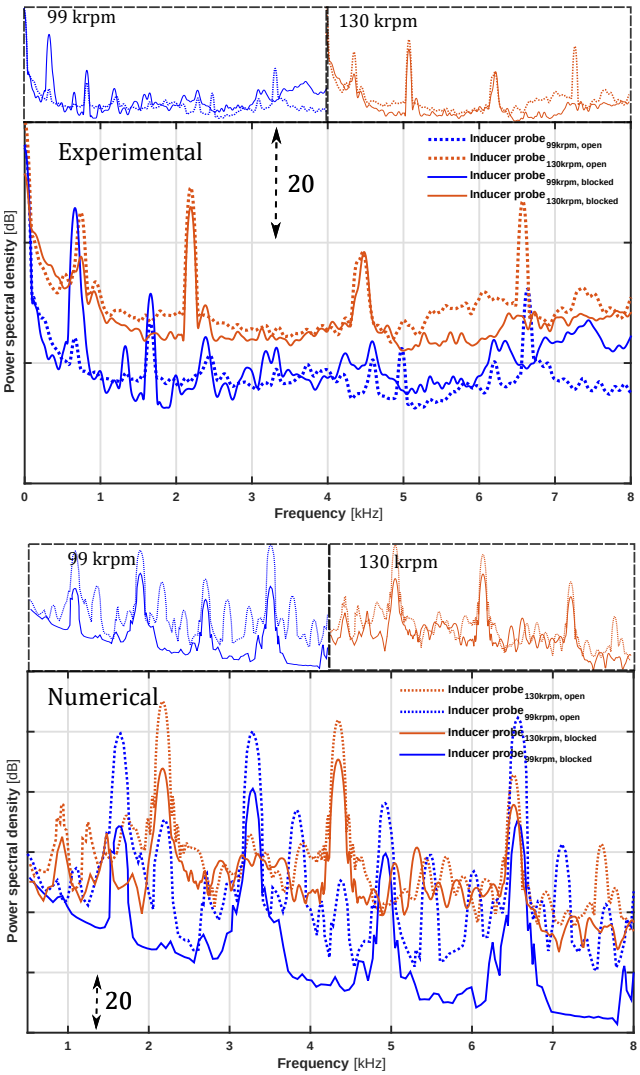

Figure 12. Experimental (top) and numerical (bottom) spectra of inducer probe for open (dashed) and blocked (solid) compressor configurations operating at the respective design conditions of 99 krpm (blue) and 130 krpm (orange) speedline. For clarity, the comparison of the open and blocked configurations are shown separately for each speedline in the inset figures.

Acoustic characteristics

The evolution of the generation and propagation of noise at the design conditions with an increase in the operating speed is quantified with the help of inducer/diffuser probes and inlet/outlet duct probes respectively. The inducer spectra of the two speedlines are shown in Fig. 12 with the experimental results of the open and blocked configurations for both speedlines shown in the top half of the figure while the predicted spectra are presented in the bottom half of the figure. Significantly higher overall levels are observed in the inducer spectra of the higher speedline for both configurations, including intense RO tones corresponding to higher Mach numbers as shown in the flow characteristics. It is interesting to observe a peak in the region of 0.65-0.75 kHz corresponding to 0.4 RO and 0.3 RO of the 99 krpm and 130 krpm speedlines respectively. This tonal feature is dominant in the spectra of the blocked configuration for the 99 krpm speedline while the spectra of the open configuration show it accentuated for the 130 krpm speedline. As observed in the comparison between the open and blocked configurations, the propagation of tonal content via the PS cavity makes the open configuration noisier, specifically for the higher speedline. Although the already established limitations of the numerical model in terms of heightened tonal content and discrepancies in the overall levels and decay rates are observed, the predicted spectra reasonably capture the impact of operational speed. The multiple tones observed in

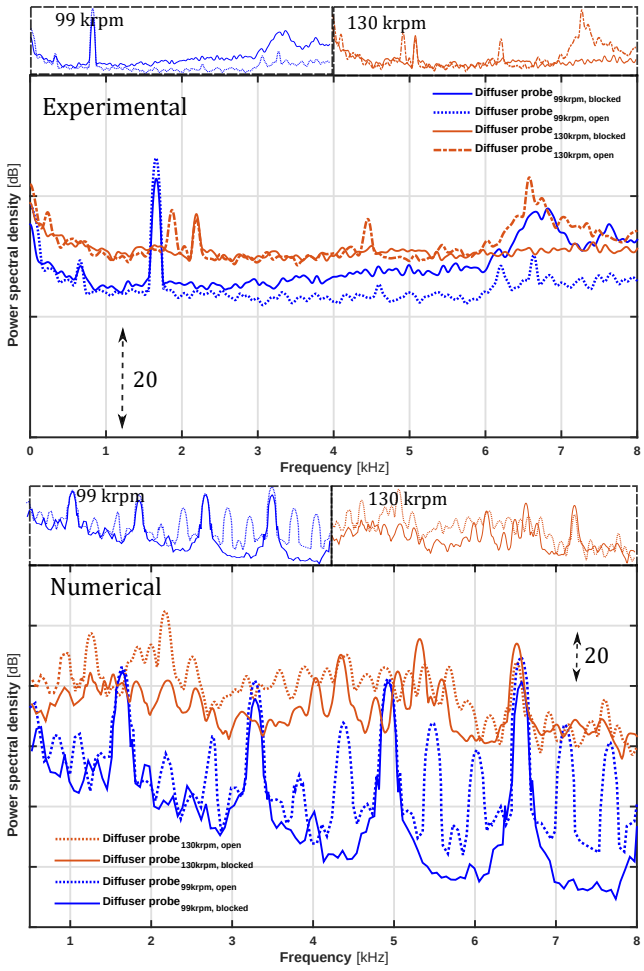

Figure 13. Experimental (top) and numerical (bottom) spectra of diffuser probe for open (dashed) and blocked (solid) compressor configurations operating at the respective design conditions of 99 krpm (blue) and 130 krpm (orange) speedline. For clarity, the comparison of the open and blocked configurations are shown separately for each speedline in the inset figures.

the predicted spectra are expected to be caused by the presence of standing waves. Unfortunately, non-reflecting boundary conditions and 'sponge zones' were not used and their implementation is expected to alleviate the issues of spurious tones in predicted spectra.

The diffuser spectra for the two speedlines are presented in Fig. 13 with the measured spectra being shown in the top half of the figure while predicted spectra are presented in the bottom half of the figure. Similar to the inducer spectra, the measured diffuser spectra for both configurations are observed to yield higher overall levels with an increase in rotational speed. Broadband elevation in the region of 6-7.5 kHz observed in the spectrum of blocked configuration operating at lower speedline is identified in the spectrum of the open configuration for the higher speedline. In the lower speedline, the diffuser spectrum of the blocked configuration is observed to yield significantly higher overall levels, whereas the spectra of the open and blocked configurations at higher speedline are similar. The numerical model is unable to accurately predict the trends observed in the measured diffuser spectra. The acoustic sources in the diffuser are expected to be dominated by the local non propagative aerodynamic disturbance field components instead of propagative fluid compressibility components and thereby, necessitating the use of a high fidelity turbulence model for accurately computing the noise generation.

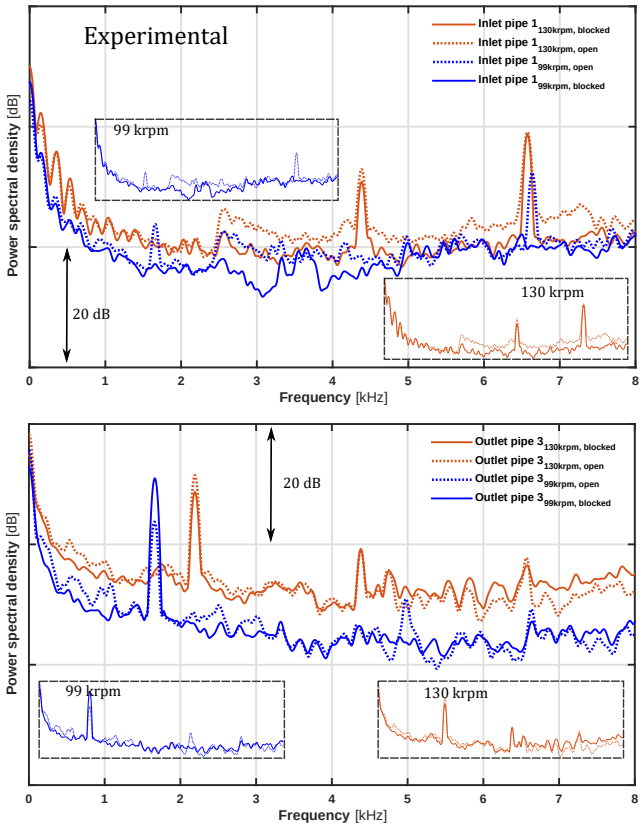

Figure 14. Experimental spectra of the inlet (top) and outlet (bottom) duct for open (dashed) and blocked (solid) compressor configurations operating at the respective design conditions of 99 krpm (blue) and 130 krpm (orange) speedline. Y-axis scale is maintained at 20 dB per division. For clarity, the comparison of the open and blocked configurations are shown separately for each speedline in the inset figures.

The propagation of noise at the inlet and the outlet ducts for two speedlines is compared in Fig. 14. Again, the overall levels for both inlet and outlet duct spectra are seen to increase with an increase in the operational speed. Similar to the inducer spectra, the noise at the inlet duct of the open configuration is observed to be higher than for the inlet duct of the blocked configuration, and this deviation between the spectra of two configurations is also higher for the higher speedline.

The outlet duct spectra for the open and blocked configurations are similar for both speedlines.

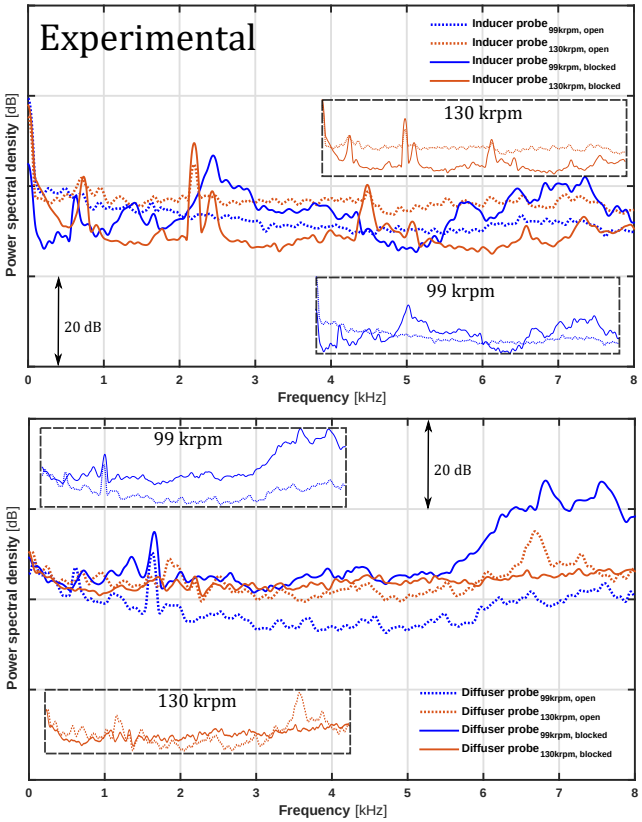

Figure 15. Experimental spectra of inducer probe (top) and diffuser (bottom) probe for open (dashed) and blocked (solid) compressor configurations operating at the respective near surge conditions of 99 krpm (blue) and 130 krpm (orange) speedline. Y-axis scale is maintained at 20 dB per division. For clarity, the comparison of the open and blocked configurations are shown separately for each speedline in the inset figures.

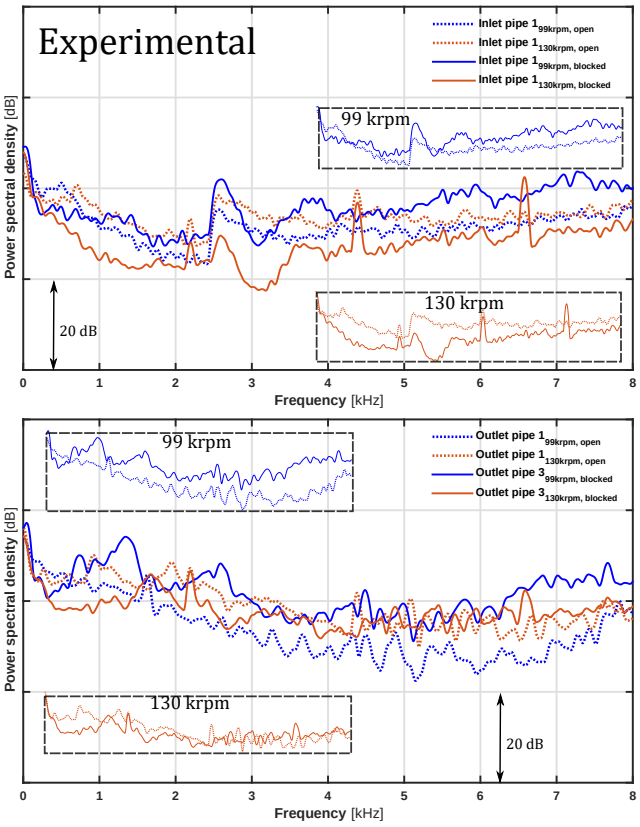

Figure 16. Experimental spectra of the inlet (top) and outlet (bottom) duct for open (dashed) and blocked (solid) compressor configurations operating at the respective near surge conditions of 99 krpm (blue) and 130 krpm (orange) speedline. Y-axis scale is maintained at 20 dB per division. For clarity, the comparison of the open and blocked configurations are shown separately for each speedline in the inset figures.

Evolution for near surge operation

As mentioned before, the impact of operating speed on the spectra of the near surge point cannot be accurately quantified by directly comparing the near surge spectra of two speedlines as the flow coefficients are not similar. Therefore, the measured near surge spectra for two speedlines are briefly discussed in this section from the perspective of perceived noise levels for different speedlines along with the acoustic changes brought by the use of casing treatment during near surge operation.

The generation of noise quantified from the spectra of the inducer and diffuser probes for compressors operating at the two speedlines are shown in Fig. 15. For the open configuration, the near surge spectra of both inducer and diffuser probes are seen to yield higher levels of noise with an increase in operational speed. It is interesting to note that while broadband features observed in the inducer spectrum of the blocked configuration for the lower speedline increases the overall noise levels, the opposite is observed in the spectra of the higher speedline. The inducer spectrum of the blocked configuration at the higher speedline shows significantly lower overall levels of noise than the open configuration and therefore, could explain the comments of authors[22,23] on PS casing treatment deteriorating the acoustic emission of the compressor. This is not exactly true as higher noise levels for compressors with casing treatment are expected due to the lower mass flow rates at the surge limit. Although the purpose of the casing treatment is to push the surge limit towards lower mass flow rates, for an aerodynamically similar near surge point (99 krpm speedline) the casing treatment is shown to alleviate the noise emission of the compressor[24].

The diffuser spectra of the blocked compressor at the lower speedline show significantly higher overall noise levels relative to the open configuration while the diffuser spectra of the two configurations operating at the higher speedline show similar levels. This again

shows the positive impact of casing treatment on noise generation in the compressor as, in spite of lower mass flow rates, the spectra of the open configurations are similar to the blocked configuration operating at a higher mass flow rate.

The propagation of this noise to the compressor ducts is shown in the inlet and outlet duct spectra presented in Fig. 16. For the open configuration, the inlet and outlet duct spectra shows increased noise levels at the higher operating speed (130 krpm) as observed in the inducer and diffuser spectra with lower differences in the overall levels of noise between the two speedlines. Similar to the in-compressor probes, the duct spectra for the blocked configurations show higher noise levels at the lower speedline while lower overall noise levels are observed for the higher speedline. These lower overall noise levels for the blocked configuration are again expected to be caused by the higher mass flow rate for the surge limit as compared to the open configuration.

Conclusions

In this investigation, the evolution of flow and acoustic features with an increase in the operational speed of a compressor were investigated by studying the operation of the compressor at the 99 krpm and 130 krpm speedlines. The computationally optimal numerical configuration using the SBES formulation on a grid with 10 million cells and a timestep corresponding to 4° impeller rotation per iteration was used in this work. Boundary conditions were obtained through experimental testing of the selected compressor configurations. Experimental data was also used to validate the numerical model performance, demonstrating a deviation of around 4 % with respect to measurements of total-to-total pressure ratio and isentropic efficiency.

Notwithstanding the limitations of the numerical configuration, the numerical spectra were shown to capture the dominant deviations between the two speedlines for the investigated configurations operating at design conditions. Although the increase in operational speed was shown to generally increase the overall acoustic emission of the compressor for both configurations, particular care should be exercised to interpret the results of near surge operation as the points were not aerodynamically similar.

For the design operation, an increase in the velocity, pressure, Mach number and entropy were observed with the increase in the operational speed. The acoustic spectra of inducer and diffuser probes showed greater noise generation at the higher speedline for both configurations. A similar trend of higher noise levels at the higher speedline was also be observed in the inlet and outlet duct spectra. The differences among the impeller-upstream (inducer and inlet duct) spectra for the open and blocked configurations were seen to increase at the higher speedline while the deviation in the diffuser and outlet duct spectra of the two configurations decreased at the higher speedline.

For the near surge operation, the impact of operating speed cannot be established by directly comparing the spectra of the two speedlines. The blocked configuration at the higher speed was observed to yield lower overall levels of noise relative to the open configuration as it was operating at a higher mass flow rate. Comparison of the near surge spectra of the two configurations operating at aerodynamically similar points, (i.e. the near surge state of the 99 krpm speedline) showed the positive impact of casing treatment on the acoustic emission by lowering the overall noise levels.

Acknowledgements

The project was sponsored and supported by BorgWarner Turbo Systems and the Regional Growth Fund (RGF Grant Award 01.09.07.01/1789C). The authors would like to thank BorgWarner Turbo Systems for permission to publish the results presented in this paper. The support of the HPC group at the University of Huddersfield is gratefully acknowledged.

Declaration of conflicting interests

The author(s) declared no potential conflicts of interest with respect to the research, authorship, and/or publication of this article.

Nomenclature

List of symbols

T temperature (K)

$T_{\text{out},0}$ total temperature at the outlet boundary (K)

$\dot{W}$ compressor absorbed work ($\text{kgm}^2\text{s}^{-3}$)

ε relative deviation (%)

γ ratio of specific heats (−)

ϕ generic variable

$p_{\text{out},0}$ total pressure at the outlet boundary (Pa)

$\Pi_{\text{t-t}}$ total-to-total pressure ratio (-)

η_s isentropic efficiency (-)

y^+ dimensionless wall distance (-)

List of abbreviations

CFD computational fluid dynamics

DES detached eddy simulation

PIV particle-imaging velocimetry

PS ported shroud

PSD pressure spectral density (dB)

RBM rigid body motion

RO rotating tone

SBES stress-blended eddy simulation

TCN tip clearance noise

References

1. Macdougal I and Elder R. The improvement of operating range in a small, high speed, centrifugal compressor using casing treatment. In IMechE Conference on Turbochargers and Turbocharging, Paper. The Institution of Mechanical Engineers, pp. 19–26.
2. Eynon P, Whitfield A, Firth M et al. A study of the flow characteristics in the inducer bleed slot of a centrifugal compressor. In ASME 1996 International Gas Turbine and Aeroengine Congress and Exhibition. American Society of Mechanical Engineers. DOI:10.1115/96-GT-262.
3. Fisher F. Application of map width enhancement devices to turbocharger compressor stages. Technical report, SAE Technical Paper, 1988. DOI:10.4271/880794.
4. Semlitsch B, JyothishKumar V, Mihaescu M et al. Numerical flow analysis of a centrifugal compressor with ported and without ported shroud. Technical report, SAE Technical Paper, 2014. DOI:10.4271/2014-01-1655.
5. Christou GA. Fluid mechanics of ported shroud centrifugal compressor for vehicular turbocharger applications. Thesis, 2015. URL http://hdl.handle.net/1721.1/101492.
6. Yang M, Martinez-Botas R, Zhang Y et al. Effect of self-recirculation-casing treatment on high pressure ratio centrifugal compressor. Journal of Propulsion and Power 2016; 32(3): 602–610. DOI:10.2514/1.B35438.
7. Zheng X, Sun Z, Kawakubo T et al. Experimental investigation of surge and stall in a turbocharger centrifugal compressor with a vaned diffuser. Experimental Thermal and Fluid Science 2017; 82: 493–506. DOI:10.1016/j.expthermflusci.2016.11.036.
8. He X and Zheng X. Roles and mechanisms of casing treatment on different scales of flow instability in high pressure ratio centrifugal compressors. Aerospace Science and Technology 2019; 84: 734–746. DOI:10.1016/j.ast.2018.10.015.
9. Torregrosa A, Broatch A, Margot X et al. Local flow measurements in a turbocharger compressor inlet. Experimental Thermal and Fluid Science 2017; 88: 542–553. DOI:10.1016/j.expthermflusci.2017.07.007.
10. Torregrosa A, García-Cuevas LM, Inhestern LB et al. Radial turbine sound and noise characterisation with acoustic transfer matrices by means of fast one-dimensional models. International Journal of Engine Research 2019; DOI:10.1177/1468087419889429.
11. Sharma S, Broatch A, Garcıa-Tıscar J et al. Acoustic characteristics of a ported shroud turbocompressor operating at design conditions. International J of Engine Research 2018; 1: 15. DOI:10.1177/1468087418814635.
12. Sharma S, Broatch A, García-Tíscar J et al. Acoustic and pressure characteristics of a ported shroud turbocompressor operating at near surge conditions. Applied Acoustics 2019; 148: 434–447. DOI:10.1016/j.apacoust.2019.01.005.
13. Broatch A, García-Tíscar J, Roig F et al. Dynamic mode decomposition of the acoustic field in radial compressors. Aerospace Science and Technology 2019; 90: 388–400. DOI:10.1016/j.ast.2019.05.015.
14. Evans D and Ward A. Minimising turbocharger whoosh noise for diesel powertrains. Technical report, SAE Technical Paper, 2005. DOI:10.4271/2005-01-2485.
15. Trochon EP. A new type of silencers for turbocharger noise control. Technical report, SAE Technical Paper, 2001. DOI:10.4271/2001-01-1436.
16. Teng C and Homco S. Investigation of compressor whoosh noise in automotive turbochargers. SAE International Journal of Passenger Cars-Mechanical Systems 2009; 2(2009-01-2053): 1345–1351. DOI:10.4271/2009-01-2053.
17. Figurella N, Dehner R, Selamet A et al. Noise at the mid to high flow range of a turbocharger compressor. Noise

Control Engineering Journal 2014; 62(5): 306–312. DOI: 10.3397/1/376229.

18. Raitor T and Neise W. Sound generation in centrifugal compressors. Journal of Sound and Vibration 2008; 314(3): 738–756. DOI:10.1016/j.jsv.2008.01.034.
19. Tiikoja H, Rämmal H, Abom M et al. Investigations of automotive turbocharger acoustics. SAE International Journal of Engines 2011; 4(2): 2531–2542. DOI:10.4271/2011-24-0221.
20. Broatch A, Galindo J, Navarro R et al. Methodology for experimental validation of a CFD model for predicting noise generation in centrifugal compressors. International Journal of Heat and Fluid Flow 2014; 50: 134–144. DOI:10.1016/j.ijheatfluidflow.2014.06.006.
21. Sharma S, Garcıa-Tıscar J, Allport JM et al. Evaluation of modelling parameters for computing flow-induced noise in a small high-speed centrifugal compressor. Aerospace Science and Technology 2020; 98: 105697. DOI:10.1016/j.ast.2020.105697.
22. Chen H and Yin J. Turbocharger compressor development for diesel passenger car applications. In IMechE Eighth International Conference on Turbochargers and Turbocharging, London, May. pp. 17–18. DOI:10.1016/B978-1-84569-174-5.50005-1.
23. Chen H and Lei VM. Casing treatment and inlet swirl of centrifugal compressors. Journal of Turbomachinery 2013; 135(4): 041010.
24. Sharma S, García-Tíscar J, Allport J et al. Effects of ported shroud casing treatment on the acoustic and flow behaviour of a centrifugal compressor. International Journal of Engine Research 2019; DOI: 10.1177/1468087419880431.
25. Sharma S, Broatch A, García-Tíscar J et al. Acoustic characterisation of a small high-speed centrifugal compressor with casing treatment: An experimental study. Aerospace Science and Technology 2019; DOI: 10.1016/j.ast.2019.105518.
26. Sharma S, García-Tíscar J, Allport JM et al. Impact of impeller casing treatment on the acoustics of a small high speed centrifugal compressor. In ASME Turbo Expo 2018: Turbomachinery Technical Conference and Exposition. American Society of Mechanical Engineers Digital Collection. DOI:10.1115/GT2018-76815.
27. Torregrosa AJ, Broatch A, Margot X et al. Experimental methodology for turbocompressor in-duct noise evaluation based on beamforming wave decomposition. Journal of Sound and Vibration 2016; 376: 60–71. DOI: 10.1016/j.jsv.2016.04.035.
28. Dehner R, Selamet A, Steiger M et al. The Effect of Ported Shroud Recirculating Casing Treatment on Turbocharger Centrifugal Compressor Acoustics, volume 10. 2017. DOI:10.4271/2017-01-1796.
29. CFX-Solver A. Theory guide. Release ll 2006; .
30. Song K, Zhao B, Sun H et al. A physics-based zero-dimensional model for the mass flow rate of a turbocharger compressor with uniform/distorted inlet condition. International Journal of Engine Research 2018; DOI:10.1177/1468087418773673.
31. Broatch A, Margot X, García-Tíscar J et al. Impact of simple surge-enhancing inlet geometries on the acoustic behavior of a turbocompressor. International Journal of Engine Research 2018; DOI:10.1177/1468087418784125.
32. Welch P. The use of fast fourier transform for the estimation of power spectra: A method based on time averaging over short, modified periodograms. IEEE Transactions on Audio and Electroacoustics 1967; 15(2): 70–73. DOI:10.1109/TAU.1967.1161901.
33. Menter F. Stress-blended eddy simulation (sbes)—a new paradigm in hybrid rans-les modeling. In Symposium on Hybrid RANS-LES Methods. Springer, pp. 27–37.
34. Gelfand SA. Essentials of audiology. New York: Thieme, 2007, 2007.
35. ANSYS I and ANSYS I. Cfd help manual. ANSYS, Inc, Canonsburg, PA 2012; .
36. Sharma S, Jupp ML, Nickson AK et al. Ported shroud flow processes and their effect on turbocharger compressor operation. In ASME Turbo Expo 2017: Turbomachinery Technical Conference and Exposition. American Society of Mechanical Engineers, pp. V02CT44A017–V02CT44A017. DOI:10.1115/GT2017-63678.